Size scaling in collective cell growth

Rocky Diegmiller[1,3], Caroline A. Doherty[2,3], Tomer Stern[2,3], Jasmin Imran Alsous[1,3,4], Stanislav Y. Shvartsman[2,3,4,*]

[1] Department of Chemical and Biological Engineering, Princeton University, Princeton, NJ 08544, USA
[2] Department of Molecular Biology, Princeton University, Princeton, NJ 08544, USA
[3] Lewis-Sigler Institute for Integrative Genomics, Princeton University, Princeton, NJ 08544, USA
[4] Flatiron Institute, Simons Foundation, New York, NY 10010, USA

*(Email: stas@princeton.edu)

Abstract

Size is a fundamental feature of living entities and is intimately tied to their function. Scaling laws, which can be traced to D'Arcy Thompson and Julian Huxley, have emerged as a powerful tool for studying regulation of the growth dynamics of organisms and their constituent parts. Yet throughout the 20th century, as scaling laws were established for single cells, quantitative studies of the coordinated growth of multicellular structures have lagged, largely due to technical challenges associated with imaging and image processing. Here, we present a supervised learning approach for quantifying the growth dynamics of germline cysts during oogenesis. Our analysis uncovers growth patterns induced by the groupwise developmental dynamics among connected cells, and differential growth rates of their organelles. We also identify inter-organelle volumetric scaling laws, finding that nurse cell growth is linear over several orders of magnitude. Our approach leverages the ever increasing quantity and quality of imaging data, and is readily amenable for studies of collective cell growth in other developmental contexts, including early mammalian embryogenesis and germline development.

Keywords: supervised learning, developmental dynamics, multicellular clusters, allometry, oogenesis

Summary Statement

Diegmiller et al. present a new approach for automating 3D reconstructions of multicellular structures and highlight its utility by analyzing patterns of growth present during *Drosophila* oogenesis.

Introduction

Uncovering the patterns and the mechanisms underlying the growth of organisms has been a longstanding goal in Biology. Propelled by D'Arcy Thompson's and Julian Huxley's seminal work over a century ago, scientists have since devised increasingly sophisticated methods to capture and analyze growth in its many forms and at scales that span a large dynamic range (Thompson (1917); Huxley (1932); Sharpe (2017)). In particular, numerous studies have focused on uncovering growth dynamics of cells and their substructures; cells are the primary building blocks of more complex structures, and the proper physical dimensions of a cell and relative sizes of its organelles are important for proper structure and function (Chan and Marshall (2010; 2013); Jorgensen et al.(2007); Neumann and Nurse (2007); Levy and Heald (2012); Marshall et al. (2012); Ginzberg et al. (2016)). Prior work, primarily focusing on *X. laevis* and *C. elegans*, has provided many of the established quantitative methods for characterizing size regulation and scaling in single cells, thus elucidating how these features regulate key biological processes, such as the cell cycle (Arata et al. (2015); Arata and Takagi (2019); Jevti´c and Levy (2015); Levy and Heald (2010); Masui and Wang(1998); Wang et al. (2016)).

In contrast to studies of growth of individual cells, studies of coordinated growth in multicellular clusters have been slow to emerge (Macklin (2019)). A particularly important class of multicellular growth problems arises during the development of gametes: Across species, oocytes and sperm develop within clusters of connected cells, called germline cysts (Pepling et al. (2015); Matova and Cooley (2001); Woznica et al. (2016); Yamashita (2018)). These structures have a relatively few number of cells (several to tens) and are conserved, thus providing a highly tractable and and relevant system for studying the growth dynamics of cells in a multicellular context. With the ever-increasing power of modern technologies and emergence of machine learning, it has now become possible to systematically analyze large data sets, to extract three-dimensional measurements of cells and their substructures, and to identify the relationships characterizing the coordinated growth of these multicellular structures, and their underlying mechanisms (Sommer et al. (2011); Machado et al. (2019); Zhang et al. (2019); Tokuoka et al. (2020)).

Here we study collective growth during invertebrate oogenesis, during which a small number of connected support cells grow rapidly and significantly, while synthesizing the molecules and molecular machines required for supporting the oocyte's growth and early embryonic life (Matova and Cooley (2001); Haglund et al. (2011); Lei and Spradling (2016)). To determine whether there are laws that govern the growth of clusters of connected cells, we focused on the *Drosophila* egg chamber, a powerful and relevant experimental system whose invariant structure allows identification and unique labeling of each cell in the cyst. An egg chamber comprises 16 germline cells enveloped by an epithelium (Fig. 1A) (Koch and King (1969); King (1970)). The germline cyst arises from a differentiated stem cell that undergoes four rounds of cell division with incomplete cytokinesis, leaving cells connected through stabilized intercellular bridges, or ring canals (King (1970); Mahajan-Miklos and Cooley (1994)). At ~ 1-10 microns, ring canals allow for intercellular communication and transport – processes that are essential for oocyte development and growth (Cooley and Theurkauf (1994)). One of the two cells with four ring canals becomes the oocyte, while the remaining 15 cells become supporting nurse cells (King (1970); Diegmiller et al. (2021)).

Over the course of 3 days, the egg chamber grows by four orders of magnitude; however, that volume increase is not partitioned equally among its 16 cells (King (1970)). While the oocyte becomes transcriptionally quiescent, the nurse cells undergo ~ 8-10 endoreplication cycles that significantly increase their ploidy, thus enabling them to synthesize the materials

necessary for future developmental events (Edgar and Orr-Weaver (2001); Fox and Duronio (2013); Navarro-Costa et al. (2001); Doherty et al. (2021)). Furthermore, studies have shown that within the nurse cell cluster itself, a hierarchy of cell sizes emerges (Brown and King (1964); Dapples and King (1970); Imran Alsous et al. (2017; 2018)). Nurse cell nuclear volumes increase with increasing ploidy, but the nurse cells also grow in concert with the oocyte; it is therefore unclear how the nuclei and cells scale during egg chamber development. Nucleolar size has been shown to correlate with ribosomal density, which is linked to cell growth rates (Rudra and Warner (2004); Uppaluri et al. (2016)); however, given the syncytial nature of these cell clusters and the ability of RNA and protein products to be exchanged within nurse cells and between nurse cells and the oocyte through ring canals, it is not clear whether each nurse cell nucleolus scales with the size of its own nucleus.

We therefore sought to investigate the coordinated growth of germline cells and their substructures during *Drosophila* oogenesis, using a high-throughput, data-driven approach. This paper was largely inspired by the previous work of Dr. Charles Dapples and Dr. Robert King, who nearly fifty years ago analyzed the shapes and volumes of nuclei and nucleoli in developing egg chambers (Dapples and King (1970)). Motivated to overcome the limitations of 2D studies, researchers of the King lab at Northwestern University set out to generate 3D visualizations of these organelles (Charles C. Dapples, personal communication). Armed with cutting-edge electron microscopy equipment at the time, the researchers began by serially sectioning through an entire egg chambers, manually tracing each acquired electron micrograph onto graph paper, and mapping the locations of nucleolar regions. For each of the ~ 50-100 micrographs obtained for each cell, this information was transferred to punch cards and fed into a computer, creating a 3D array of the nucleolar region. This laborious process required months to complete; furthermore, the resolving power of the micrographs limited the statistical power and scope of this study. Nonetheless, these efforts yielded the first insights into the unique 3D structure of this organelle (Fig. 1B).

Technology has come far since, yet to obtain measurements of cell volumes, numerous studies still assume that cells are spherical objects, or rely on interpolation of circular areas across slices (Arata et al. (2015); Arata and Takagi (2019); Masui and Wang (1998); Wang et al. (2016)). The approach presented in this paper allowed us to determine the morphological features and to measure the volumes of cells and their organelles for each cell in egg chambers across several orders of magnitude, while circumventing these limitations. Our results shed light on several properties relating to the groupwise developmental dynamics of these multicellular clusters. More generally, this work establishes an automated pipeline for high-throughput data processing and systematic analysis that is unencumbered by large data sets and can be readily applied to characterize collective growth in a several multicellular systems, including early mammalian embryos and germline cysts.

Results and Discussion

Algorithm for automated egg chamber reconstruction

Since live imaging is limited to a few hours, we set out to establish scaling relationships in *Drosophila* egg chambers for each of the 16 cells in the germline cyst using fixed samples with fluorescently labeled cell membranes, ring canals, nuclei, and nucleoli (Materials and Methods). While formaldehyde fixation may disturb the integrity of living materials, the egg chamber's cells and substructures appeared largely unaffected (Fig. 2). Each cell in the cyst was uniquely identified using a supervised learning approach.For each of the 15 nurse cells,

the volumes of the cells, as well as their nuclei and nucleoli were measured, and their sizes reconstructed over ~60 hours of oogenesis, namely, from Stages 3 to 10A (King (1957); Spradling (1993)). This supervised learning program yielded probabilistic pixel information based on minimal training (Sommer et al. (2011); Berg et al. (2019)). Once these probability maps were exported to MATLAB to isolate each feature within each egg chamber, we were able to uniquely identify each cell in the cyst, reconstruct its morphology, measure its volume, and extract those features for its nucleus as well. The unique identification of nurse cells was made possible through implementation of an assignment algorithm relating the identified cell-cell connections based on the positions of ring canals within the system. After identifying the oocyte, each cell in the egg chamber is identifiable by the number of its ring canals and which other cells it was connected to. The automated reassignment algorithm allowed each nurse cell to be distinctly labeled in a given egg chamber and compared with the same cell in other egg chambers across developmental stages (Kuhn (1955); Umeyama (1988)). This automated pipeline for image processing and reconstruction (Fig. 2), facilitates extraction of quantitative information regarding the temporal evolution and development of the connected network of cells.

Linear scaling of nuclear and cell volumes

Discovery of the emergent pattern of cell sizes within the nurse cell cluster was first enabled through measurements from 2D sections, and subsequently confirmed through painstaking manual measurements and 3D reconstructions (Brown and King (1964); Imran Alsous et al. (2017; 2018)). These studies formed the basis for interrogating features and dynamics of cell and organelle growth through the more advanced, higher throughput, and automated computational and image processing tools featured here.

Previous works demonstrated that nuclear volumes correlate with distance from the oocyte – namely, that the number of ring canals between a nurse cell and the oocyte correlate with the nuclear volume of a cell (Brown and King (1964); Imran Alsous et al. (2017)). We first sought to verify this finding using the automated reconstructions and to expand its scope to total nurse cell volumes. We recovered a strong correlation between nurse cell volume rank and nuclear volume rank (Fig. S1A), thus validating the accuracy of the aforementioned approach and establishing an important link between previous manual reconstructions and the automated versions presented here.

Nurse cell volume fractions remain constant during growth

Previous work has also demonstrated that nurse cells exhibit differential growth, and that four groups of nurse cell sizes emerge, correlating with the cells' distance from the oocyte. This pattern of cell sizes is already present in egg chambers that have exited the germarium, the stem cell niche (Brown and King (1964); Imran Alsous et al. (2017; 2018)); furthermore, once the pattern emerges from uniform initial conditions, it persists throughout oogenesis until the onset of nurse cell dumping, when the nurse cells' volumes start to decrease markedly through rapid transport oftheir cytoplasmic contents to the oocyte (Theurkauf and Hazelrigg (1998); Imran Alsous et al. (2021)).

In addition to confirming these findings, we found that the volume fraction of each nurse cell in a given egg chamber between Stages 3 and 10A does not depend on developmental stage (Fig. S1B) (Jia et al. (2016); King (1957)). That is, the size of the eggchamber does not have predictive power for the relative nurse cell sizes. Instead, volume fractions appear to be conserved across developmental stages and are roughly uniform based on distance from the oocyte. In particular, there is a clear deviation for the four cells directly connected to the oocyte, while the other cells in the cyst appear to be more uniformly distributed. Given the nurse cells' size hierarchy, conservation of relative nurse cell volume fractions across all measured samples implies that the observed size divergence of nurse cells based on distance from the oocyte must have occurred at a time point before the earliest egg chamber measured in this study (~ Stage 3) (Jia et al. (2016); Imran Alsous et al. (2017); Doherty et al. (2021)).

Nurse cell nuclei and nucleoli grow isometrically

We next explored the total growth rates of nucleolar and nuclear regions within developing egg chambers. Starting from early ~ Stage 3 egg chambers, we found that nurse cell nuclear and nucleolar volumes scale at the same rates with respect to each other through developmental time. (Figs 3A,B) (Jia et al. (2016)). This observation is consistent with that made half a century ago by Dapples and King (Dapples and King (1970)). Across various stages of oogenesis, the relationship between nuclear and nucleolar size within each nurse cell remains consistent, scales isometrically with cell size, and is independent of distance from the oocyte or location in the cell lineage tree. Taken together, these data suggest that nurse cell nuclear volumes change at constant rates across developmental stages.

Oocyte growth diverges from nurse cell growth

While relative nurse cell growth remains constant throughout development, oocyte volume does not follow this trend. During the early stages of oogenesis (~ Stages 3 through 7-8), the oocyte grows roughly isometrically with the rest of the cells in thecyst; however, when the total egg chamber reaches a volume of roughly $10^5 \mu m^3$, oocyte growth begins to diverge, becoming much larger than the other cells in the developing cyst (Fig. 4).
We found that while nurse cells as a whole appear to have one rate of growth throughout oogenesis relative to the entire egg chamber (Fig. S1C), two distinct growth rates exist for the oocyte. This sharp increase in growth rate relative to the growth of the egg chamber occurs around Stage 9, when developmental processes such as yolk uptake take place (Spradling (1993); Jia et al. (2016)). This developmental checkpoint appears to split oocyte growth into two distinct phases: Early, isometric growth relative to the nurse cells, and later, divergent growth, where the oocyte grows at around twice the rate as the nurse cells.

Contextualizing analysis and applications to other systems

The work presented here highlights the utility and feasibility of automated reconstruction algorithms in quantifying developmental processes. The key strength of this approach is its flexibility: Given either stacks of fixed images or movies of developing multicellular

structures, a minimal amount of training on images is required before one is able to uniquely identify each cell within a given system, make quantitative measurements at varying scales, and glean insights into developmental trajectories. Wedemonstrate this approach here by quantifying the relative growth rates of oocyte, nurse cells, and their subparts in the *Drosophila* egg chamber, thus uncovering properties of their growth dynamics.

A key aspect of this analysis was comparing the growth rates of nucleoli and nuclei across development and within the nurse cell cluster. During oogenesis, ribosomal RNA are rapidly synthesized in nurse cell nucleoli (Jorgensen et al. (2007); Uppaluri et al. (2016)). As ribosomes are required for protein translation, an increase in the number of ribosomes promotes an increase in cell growth, as occurs in the nurse cells (Rudra and Warner (2004)). Since nurse cell nucleoli and nuclei grow at roughly the same rates, ribosomal density is most likely constant throughout *Drosophila* oogenesis. This observation implies that nurse cell growth rates are constant across developmental stages, consistent with our other findings. Nuclear and nucleolar sizes also scale with cell size (Fig. 3A). This relationship has been observed in a range of organisms and cell types, and implies that nuclear size is most likely regulated by cytoplasmic volume and contents (Gregory (2005); Levy and Heald (2012)).

A key feature of nucleoli in nurse cells is their "lava lamp" morphology, with the nucleolus loosely wrapped by the surrounding DNA (Fig. 3A, inset) (Dapples and King (1970)). This unusual structure is a departure from the more familiar dense, olive pit-like region observed in other cell types (Jorgensen et al. (2007); Neumann and Nurse (2007); Windner et al. (2019)). Given the nurse cells' ploidy and high biosynthetic capacity, such morphology may allow for a relatively higher surface area to volume ratio than the more compactly packed configuration – a hypothesis that can betested by applying the pipeline developed here to flies with mutations in rRNA structural gene locus, such as *bobbed* (*bb*), which is known to cause delayed development, with oogenesis progressing at significantly reduced rates (Kay and Jacobs-Lorena (1987)).

A striking feature of *Drosophila* oogenesis is the rapid growth of the egg chamber around Stage 9, which correlates with the uptake of yolk by the oocyte (Fig. 4), and cannot be accounted for by the isometric growth rates of the nurse cells (King (1970); Bownes (1982); Spradling (1993); Jia et al. (2016)). Indeed, while the oocyte and the nurse cells reside within a shared cytoplasm, they exhibit strikingly different nuclear behaviors and sizes (Fig. 1A). Future work is required to investigate the factors that control the scaling of nuclei in the egg chamber, both temporally throughout oogenesis, and spatially within the network. Notably, the egg chamber's functionally and morphologically different nuclei are reminiscent of the macro- andmicronuclei that reside within the same cell in the protozoan *Tetrahymena thermophila*, where differences in nuclear size and behavior have been attributed to differences in nuclear pore complexes (Levy and Heald (2012)).

Lastly, the presented approach can be adapted to developmental systems where the structure of intercellular connections is known and invariant, such as the tardigrade *Dactylobiotus parthenogeneticus* and the Argentine ant *Linepithema humile* (Poprawa et al. (2015); Eastin et al. (2020)). The key adjustment would only be in the application of the assignment algorithm that uniquely identifies each cell (Umeyama (1988)). As in *Drosophila*, the known matrix of connections between uniquely identifiable cells would need to be compared with that of each reconstructed sample, allowing for the proper identification and analysis of multicellular growth in a variety of developmental contexts.

Materials and Methods

Fly stocks

Fibrillarin-RFP flies were used in all studies as a marker for nucleolar regions within each nurse cell (Falahati and Wieschaus (2017)). The flies were maintained with standard cornmeal, molasses, and yeast media.

Antibody staining

Ovaries were fixed in 4% paraformaldehyde in 0.1% Tween-20 in PBS for 20 minutes at room temperature on a nutator. After washing in 0.1% Tween in PBS, the ovaries were then blocked for two hours in blocking solution (1% BSA in PBS) before adding the primary antibody rabbit anti-Phosphotyrosine (1:500) and rocked overnight at 4˚C overnight. The following secondary antibodies and additional stains were then used: donkey anti-rabbit Alexa-Fluor 647 nm (1:400) (Invitrogen), Alexa Fluor 488 phalloidin (1:1000) (Invitrogen), and DAPI (250 ng/mL).

Mounting and imaging

Dissected ovaries were mounted in a 1:1 mixture of RapiClear 1.47 (SUNJin Lab) and Aqua-Poly/Mount (Polysciences). Imaging was performed on a Leica SP5 confocal microscope using a 63x/1.3 NA oil objective. Three dimensional stacks were acquired using 405, 488, 546, and 647 nm in series with 3x line averaging. Stacks acquired were usually between 70-120 z-slices of 16-bit, 1024 x 1024 images. Each image was isometric in the x and y directions, tuned to best match the necessarily larger z-length. Most acquired images were 246 nm in x and y, and 250 nm in z. Calibration of volume measurements was performed using 1.8 micron diameter spherical beads to confirm accuracy of measurements in all three directions.

Image processing and supervised learning

Raw image stacks were pre-processed using FIJI to isolate individual egg chambers within each stack. The channels for each egg chamber were then split and recombined to create three stacks: a stack containing nuclear and nucleolar data, a stack containing ring canal data, and a stack containing cell membrane data. Multiple representative stacks for each type of data were uploaded into the Pixel Classification module for training within ilastik, a freely accessible semi-supervised machine learning program (Sommer et al. (2011); Berg et al. (2019)). For each type of data, training was performed by manually identifying pixels that belong to each class of interest. Based on a minimal number of these examples, the program then developed probabilities for each pixel ofa stack to belong to each of these classes. Due to the morphological and volumetric differences between early- and late-stage egg chambers, two sets of training data were used to more accurately identify the relevant features for each

class of samples. Each classifier was trained to identify the relevant features for all three stacks, yielding an output matrix of probabilities across all three dimensions.

Egg chamber reconstruction

The processed stacks, containing information about the probability of each pixel in the image to belong to either the cell membrane, ring canal, nucleus, nucleolus, or image background, were imported into MATLAB for final object identification, post-processing, and data quantification. Cell membrane probability maps were used to identify the areas of lowest probability lying inside the egg chamber, which were used as seeds for the watershed transformation. After applying this transformation and applying a Gaussian smoothing kernel based on the size of the image being analyzed, this process yielded the sixteen objects most likely to be the cells within the developing cyst and assign each object a unique identifier. Applying a simple probability threshold (usually taken to be 0.5, or 50% certainty for a given pixel to have come from a certain class) allowed for the ring canals, nuclear, and nucleolar regions to all be identified within the cluster. As each ring canal connected two cells in the cluster, each necessarily touched the boundary of the connected cells. Exploiting this fact allowed for an adjacency matrix to be built that contained information about which cells are connected. This was done by creating an n-by-n matrix A, where n is the number of cells, where for each pair of connected nurse cells i and j, A_{ij} and A_{ji} were set to 1. Connections between the oocyte and nurse cells were instead weighted by a factor of 2.

Identifying the oocyte required the segmentation of the nucleus and nucleolus of each cell in the cluster. Since the nuclei and nucleoli of each cell were classified in a previous step, this was performed by identifying the location of each nucleolar region and identifying which cell each region was within. Because the oocyte is transcriptionally quiescent throughout these stages of oogenesis (Edgar and Orr-Weaver (2001); Fox and Duronio (2013)), nuclear staining in this cell appears less intense, allowing it to be identified as the oocyte. Once the oocyte was properly identified, all nurse cells and their respective organelles could be uniquely identified due to the bilateral symmetry of connections within the cell cluster. This was done by applying a graph matching algorithm in which the cell-cell connections identified through ring canals were compared to the known adjacency matrix of the uniquely labeled cyst and re-allocated (Kuhn (1955); Umeyama (1988)). This matrix reallocation process is based on the Hungarian algorithm, an optimization algorithm applied in this context to find the best configuration for assigning label j from the known adjacency matrix to object i from the sample adjacencymatrix for all labels and objects. For each sample, this automatic segmentation and identification algorithm produced a set of objects from which quantitative data was obtained for further statistical analyses. Once each nurse cell was uniquely defined,volumes were measured by calculating the number of voxels within each object of interest and scaling by the voxel size in all three dimensions, thus approximating each volume as the sum of many small rectangular prisms. A subset of these samples were compared with egg chambers reconstructed manually in Imaris to confirm the absence of systematic biases in volume measurements or segmentation.

Statistical analysis

Simple linear regression was performed using standard functions in MATLAB, assuming that the relationship between two properties, x and y, could be best represented as $\ln(y) = m \ln(x) + \ln(b)$. Rearranging these relationships yields the relationship $y = bx^m$, which shows that the slope of the regression, m, is the scaling factor between the two properties.

Acknowledgements
The authors thank Gary Laevsky for help and expertise throughout this work and acknowledge the Molecular Biology Confocal Imaging Facility, which is a Nikon Center of Excellence. The authors additionally recognize Li Cao and Maysam Shahedi for open-source MATLAB codes implementing the Hungarian algorithm (Cao, `munkres`) and helpful visualization (Shahedi, `imagesc3D`). In addition, the authors also thank Eric Wieschaus, Trudi Schüpbach, and Charles Dapples for helpful discussions.

Competing interests
The authors declare no competing or financial interests.

Contribution
S.Y.S designed the project; R.D. and C.A.D. conducted experiments; R.D. acquired images and classified training algorithms; R.D. and T.S. developed codes; C.A.D. performed manual reconstructions; R.D. analyzed data; R.D., C.A.D., T.S., J.I.A., and S.Y.S. wrote the manuscript.

Funding
This work was supported by the National Institutes of Health [F31HD098835 to R.D., R01GM134204 to S.Y.S.] and the European Molecular Biology Organization [ALTF 215-2017 to T.S.].

Data availability
All MATLAB codes used in this study have been made available at `https://github.com/Shvartsman-Lab/EggChamberScaling`. Sample input image stacks, ilastik training sets and output files for these codes will be made available upon request.

Supplementary
Supplementary information available online at:

References

Arata, Y., Takagi, H., Sako, Y., and Sawa, H. (2015). Power law relationship between cell cycle duration and cell volume in the early embryonic development of *Caenorhabditis elegans*. *Front. Physiol.* **5**, 529.

Arata, Y. and Takagi, H. (2019). Quantitative studies for cell-division cycle control. *Front. Physiol.* **10**, 1022.

Berg, S., Kutra, D., Kroeger, T., Straehle, C. N., Kausler, B. X., Haubold, C., Schiegg, M., Ales, J., Beier, T., Rudy, M., et al. (2019). ilastik: interactive machine learning for (bio)image analysis. *Nat. Meth.* **16**, 1226–1232.

Bownes, M. (1982). Hormonal and genetic regulation of vitellogenesis in *Drosophila*. *Q. Rev. Biol.* **57**, 247–274.

Brown, E. H. and King, R. C. (1964). Studies on the events resulting in the formation of an egg chamber in *Drosophila melanogaster*. *Growth* **28**, 41–81.

Chan, Y. H. and Marshall, W. F. (2010). Scaling properties of cell and organelle size. *Organogenesis* **6**, 88–96.

Chan, Y. H. and Marshall, W. F. (2013). How cells know the size of their organelles. *Science* **337**, 1186–1189.

Cooley, L. and Theurkauf, W. E. (1994). Cytoskeletal functions during *Drosophila* oogenesis. *Science* **266**, 590–596.

Dapples, C. C. and King, R.C. (1970). The development of the nucleolus of the ovarian nurse cell of *Drosophila melanogaster*. *Z. Zellforsch.* **103**, 34–47.

Diegmiller, R., Zhang, L., Gameiro, M., Barr, J., Imran Alsous, J., Schedl, P., Shvartsman, S. Y., and Mischaikow, K. (2021). Mapping parameter spaces of biological switches. *PLoS Comp. Biol.* **17**, e1008711.

Doherty, C. A., Diegmiller, R., Kapasiawala, M., Gavis, E. R., and Shvartsman, S. Y. (2021). Coupled oscillators coordinate collective germline growth. *Dev. Cell* **56**, 860–870.

Eastin, K. J., Huang, A. P., and Ferree, P. M. (2020). A novel pattern of germ cell divisions in the production of hymenopteran insect eggs *Biol. Lett.* **16**, 20200137.

Edgar, B. A. and Orr-Weaver, T. L. (2001). Endoreplication cell cycles: more for less. *Cell* **105**, 297–306.

Falahati, H. and Wieschaus, E. (2017). Independent active and thermodynamic processes govern the nucleolus assembly *in vivo*. *Proc. Nat. Acad. Sci.* **114**, 1335–1340.

Fox, D. T. and Duronio, R. J. (2013). Endoreplication and polyploidy: insights into development and disease *Development* **140**, 3–12.

Ginzberg, M. B., Kafri, R., and Kirschner, M. (2016). On being the right (cell) size. *Science* **348**, 1245075.

Gregory, T. R. (2005). Genome size evolution in animals. *Evol. Genome* **1**, 3–87.

Haglund, K., Nezis, I. P., and Stenmark, H. (2011). Structure and functions of stable intercellular bridges formed by incomplete cytokinesis during development. *Commun. Integr.* **4**, 1–9.

Huxley, J. S. (1932). *Problems of Relative Growth*, New York, NY: The Dial Press.

Imran Alsous, J., Villoutreix, P., Berezhovskii, A. M., and Shvartsman, S.Y. (2017). Collective growth in a small cell network. *Curr. Biol.* **27**, 2670–2676.

Imran Alsous, J., Villoutreix, P., Stoop, N., Shvartsman, S. Y., and Dunkel, J. (2018). Entropic effects in cell lineage tree packings. *Nat. Phys.* **14**, 1016–1021.

Imran Alsous, J., Romeo, N., Jackson, J. A., Mason, F. M., Dunkel, J., and Martin, A. C. (2021). Dynamics of hydraulic and contractile wave-mediated fluid transport during *Drosophila* oogenesis *Proc. Nat. Acad. Sci.* **118**,e2019749118.

Jevtić, P. and Levy, D. L. (2015). Nuclear size scaling during *Xenopus* early development contributes to midblastula transition timing. *Curr. Biol.* **25**, 45–52.

Jia, D., Xu, Q., Xie, Q., Mio, W., and Deng, W.-M. (2016). Automatic stage identification of *Drosophila* egg chamber based on DAPI images. *Sci. Rep.-UK* **6**, 18850.

Jorgensen, P., Edgington, N. P., Schneider, B. L., Rupes, I., Typers, M., and Futcher, B. (2007). The size of the nucleus increases as yeast cells grow. *Mol. Biol. Cell* **18**, 3523–3532.

Kay, M. A. and Jacobs-Lorena, M. (1987). Developmental genetics of ribosome synthesis in *Drosophila*. *Trends Genet.* **3**, 347–351.

King, R. C. (1957). Oogenesis in adult *Drosophila melanogaster*. II. Stage distribution as a function of age *Growth* **21**, 95–102.

King, R. C. (1970). *Ovarian Development in Drosophila melanogaster*, New York, NY: Academic Press.

Koch, E. A. and King, R. C. (1969). Further studies on the ring canal system of the ovarian cystocytes of *Drosophila melanogaster*. *Z. Zellforsch.* **102**, 129–152.

Kuhn, H.W. (1955). The Hungarian method for the assignment problem *Nav. Res. Logist. Q.* **2**, 83–97.

Lei, L. and Spradling, A. C. (2016). Mouse oocytes differentiate through organelle enrichment from sister cyst germ cells. *Science* **352**, 95–99.

Levy, D. L. and Heald, R. (2010). Nuclear size is regulated by importin α and Ntf2 in *Xenopus*. *Cell* **143**, 288–298.

Levy, D. L. and Heald, R. (2012). Mechanisms of intracellular scaling. *Annu. Rev. Cell Dev. Biol.* **28**, 113–135.

Machado, S., Mercier, V. and Chiaruttini, N. (2019). LimeSig: a coarse-grained lipid membrane simulation for 3D image segmentation. *BMC Bioinformatics* **20**, 2.

Macklin, P. (2019). Key challenges facing data-driven multicellular systems biology. *GigaScience* **8**, 1–8.

Mahajan-Miklos, S. and Cooley, L. (1994). Intercellular cytoplasm transport during *Drosophila* oogenesis. *Dev. Biol.* **165**, 336–351.

Marshall, W. F., Young, K. D., Swaffer, M., Wood, E., Nurse, P., Kimurs, A., Frankel, J., Wallingford, J., Walbot, V., Qu, X. et al. (2012). What determines cell size? *BMC Biol.* **10**, 101.

Masui, Y. and Wang, P. (1998), Cell cycle transition in early embryonic development of *Xenopus laevis*. *Biol. Cell* **90**, 537–548.

Matova, N. and Cooley, L. (2001), Comparative aspects of animal oogenesis. *Dev. Biol.* **231**, 291–320.

Navarro-Costa, P., McCarthy, A., Prudêncio, P., Greer, C., Guilhur, L. G., Becker, J. D., Secombe, J., Rangan, P., and Martinho, R. G. (2016), Early programming of the oocyte epigenome controls late prophase I transcription and chromatin remodelling. *Nat. Commun.* **7**, 12331.

Neumann, F. R. and Nurse, P. (2007). Nuclear size control in fission yeast. *J. Cell Biol.* **179**, 593–600.

Pepling, M. E., de Cuevas, M., and Spradling, A.C. (1999). Germline cysts: a conserved phase of germ cell development? *Trends Cell Biol.* **9**, 257–262.

Poprawa, I., Hyra, M., and Rost-Roszkowska, M. M. (2015). Germ cell cluster organization and oogenesis in the tardigrade *Dactylobiotus parthenogeneticus* Bertolani, 1982 (Eutardigrada, Murrayidae) *Protoplasma* **252**, 1019–1029.

Rudra, D. and Warner, J. R. (2004). What better measure than ribosome synthesis? *Genes & Dev.* **18**, 2431–2436.

Sharpe, J. (2017). Computer modeling in developmental biology: growing today, essential tomorrow. *Development* **144**, 4214–4225.

Sommer, C., Straehle, C., Köthe, U., and Hamprecht, F. A. (2011). Ilastik: interactive learning and segmentation toolkit. *2011 IEEE International Symposium on Biomedical Imaging: From Nano to Macro*, Chicago, IL, 230–233.

Spradling, A. C. (1993). Developmental genetics of oogenesis. In *The Development of* Drosophila melanogaster (ed. M. Bate and A. Martinez-Arias), pp. 1–70. Cold Spring Harbor, NY: Cold Spring Harbor Laboratory Press.

Theurkauf, W. E. and Hazelrigg, T. I. (1998). *In vivo* analyses of cytoplasmic transport and cytoskeletal organization during *Drosophila* oogenesis: characterization of a multi-step anterior localization pathway. *Development* **125**, 3655-3666.

Thompson, D. W. (1917). *On Growth and Form*, Cambridge, UK: Cambridge University Press.

Tokuoka, Y., Yamada, T. G., Mashiko, D., Ikeda, Z., Hiroi, N. F., Kobayashi, T. J., Yamagata, K., and Funahashi, A. (2020). 3D convolutional neural networks-based segmentation to acquire quantitative criteria of the nucleus during mouse embryogenesis. *npj Systems Biology and Applications* **6**, 32.

Umeyama, S. (1988). An eigendecomposition approach to weighted graph matching problems. *IEEE Transactions on Pattern Analysis and Machine Intelligence* **10**, 695–703.

Uppaluri, S., Weber, S. C., and Brangwynne, C. P. (2016). Hierarchical Size Scaling during Multicellular Growth and Development. *Cell Rep.* **17**, 345–352.

Windner, S. E., Manhart, A., Brown, A., Mogilner, A., and Baylies, M. K. (2019). Nuclear scaling is coordinated among individual nuclei in multinucleated muscle fibers. *Dev. Cell* **49**, 1–15.

Wang, P., Hayden, S., and Masui, Y. (2000). Transition of the blastomere cell cycle from cell size-independent to size-dependent control at the midblastula stage in *Xenopus laevis*. *J. Exp. Zool.* **287**, 128–144.

Woznica, A., Cantley, A. M., Beemelmanns, C., Freinkman, E., Clardy, J., and King, N. (2016). Bacterial lipids activate, synergize, and inhibit a developmental switch in choanoflagellates. *P. Natl. Acad. Sci. USA.* **113**, 7894–7899.

Yamashita, Y. M. (2018). Subcellular specialization and organelle behavior in germ cells. *Genetics* **208**, 19–51.

Zhang, Y., Mesaros, A., Fujita, K., Edkins, S. D., Hamidian, M. H., Ch'ng, K., Eisaki, H., Uchida, S., Davis, J. C. S., Khatami, E. et al. (2019). Machine learning in electronic-quantum-matter imaging experiments. *Nature* **570**, 484–490.

Figures

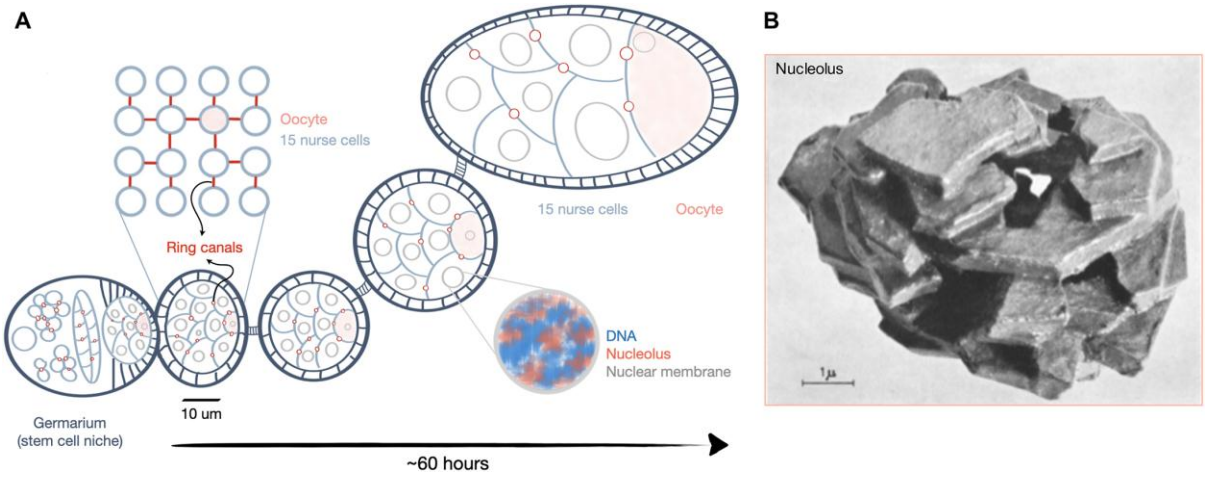

Figure 1. Schematic of *Drosophila* egg chamber development. (A) The *Drosophila* ovariole comprises a germarium and several egg chambers arranged from youngest (left) to oldest (right). The egg chamber is formed in the germarium where a differentiated stem cell undergoes four rounds of divisions to give rise to a 16-cell cyst, whose cells are connected through ring canals. The cells' stereotypic connectivity is illustrated as a network of nodes (cells) and edges (ring canals); one cell (pink) is specified as the oocyte, while the other 15 become endoreplicating nurse cells. Over time, the egg chamber grows by several orders of magnitude, with the oocyte eventually occupying a large fraction of the egg chamber volume. During this time, nurse cell nuclear and nucleolar volumes grow as the nurse cells undergo several rounds of DNA replication. (B) An early 3D model of a Stage 9 nurse cell nucleolus reconstructed from thick cardboard, depicting its intricate morphology (reproduced with permission from Dapples and King (1970)).

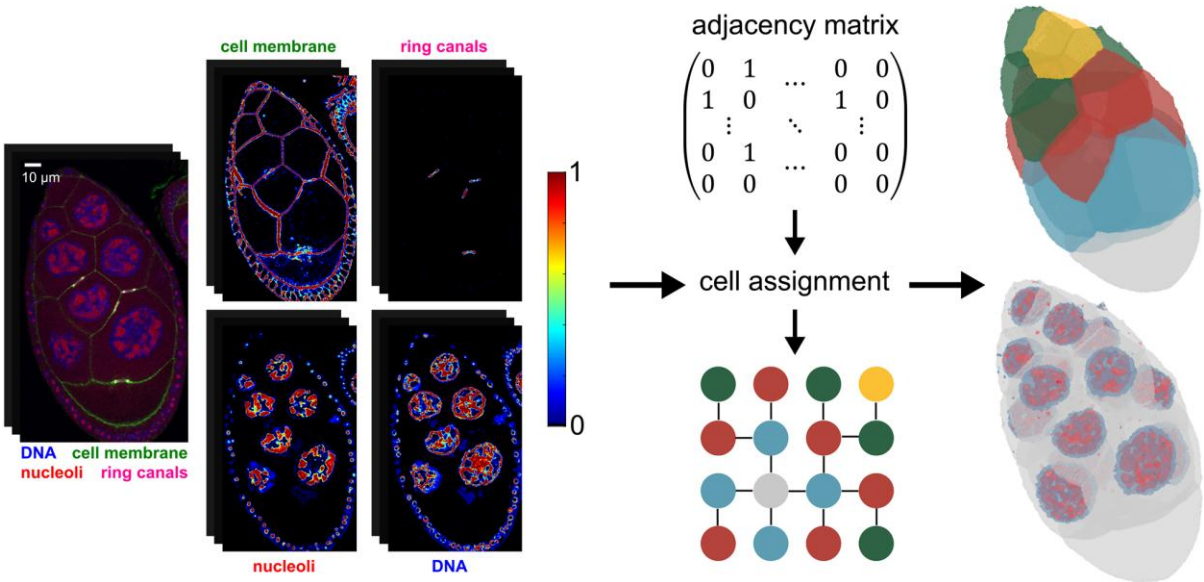

Figure 2. Pipeline for automated egg chamber reconstruction. Fixed stacks of images were stained for cell membrane, ring canals, DNA, and nucleoli. From here, training in ilastik was performed, where each pixel in a given stack was assigned a list of probabilities for being a member of each of these classes (colorbar shows probability in the interval $[0,1]$ within slice for each respective feature). These probabilities were then exported to MATLAB, where cell membrane data were used to identify the 16 cells of the cyst. Using the ring canals to identify adjacent cells, each cell identified in MATLAB can be mapped one-to-one to a unique label using the known adjacencies of the invariant *Drosophila* egg chamber.

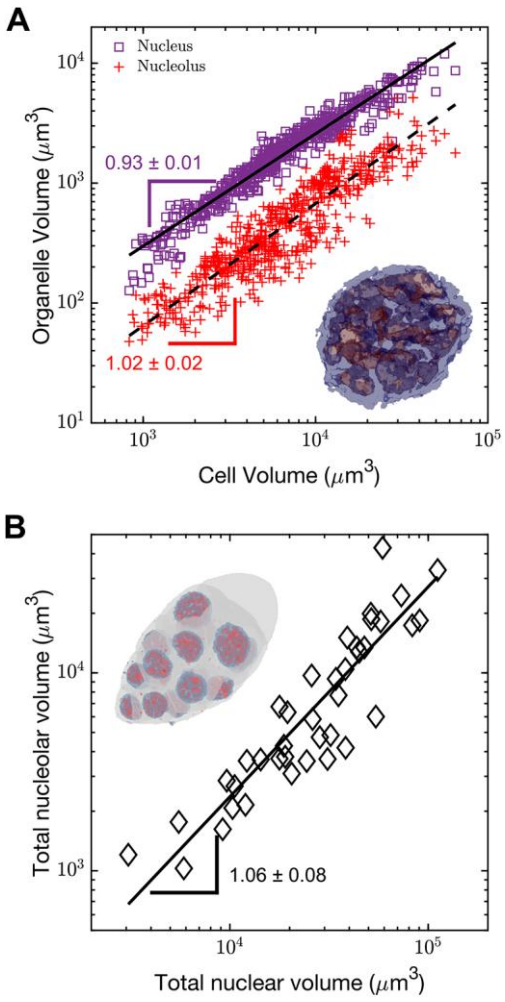

Figure 3. Subcellular scaling relationships in *Drosophila* oogenesis. (A) Nucleolar and total nuclear volumes as a function of nurse cell volume shows that these organelles grow isometrically with respect to one another ($R^2 = 0.82$ for nucleoli and $R^2 = 0.94$ for total nuclear regions). Inset is a projection of a 3D rendered nucleus, with DNA in blue and nucleolar region in red. (B) Total nucleolar volume as a function of total nuclear volume exhibits the same isometric relationship ($R^2 = 0.80$), thus recapitulating previous results (Dapples and King (1970)). Inset is a reconstructed egg chamber with the full nuclear regions of each nurse cell. For both plots, $n = 600$ nurse cells or $n = 40$ egg chambers. All slopes are given as mean ± s. d.

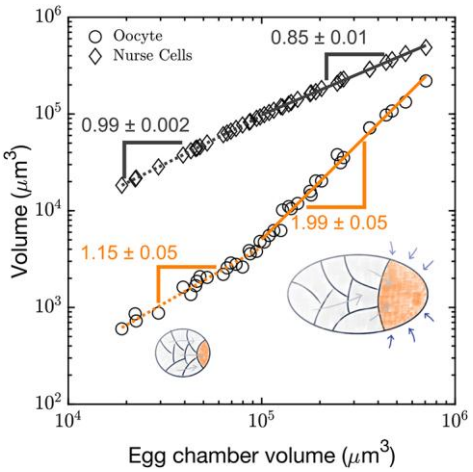

Figure 4. Divergent growth in the oocyte during oogenesis Oocyte volume and total nurse cell volume as a function of total egg chamber volume across developmental stages highlights the divergence of oocyte growth rate at a stage of oogenesis. As depicted in the schematics, this increase in the rate of growth of the oocyte relative to the growth rate of the entire egg chamber appears to come from external sources, most likely due to the onset of vitellogenesis around this stage of development. Early and late stage nurse cell growth rates relative to the egg chamber have a correlation of $R^2 = 0.999$ and $R^2 = 0.998$, respectively. Early and late stage oocyte relative growth rates have a correlation of $R^2 = 0.97$ and $R^2 = 0.99$, respectively. Here, $n = 40$ total egg chambers. All slopes are given as mean ± s. d.

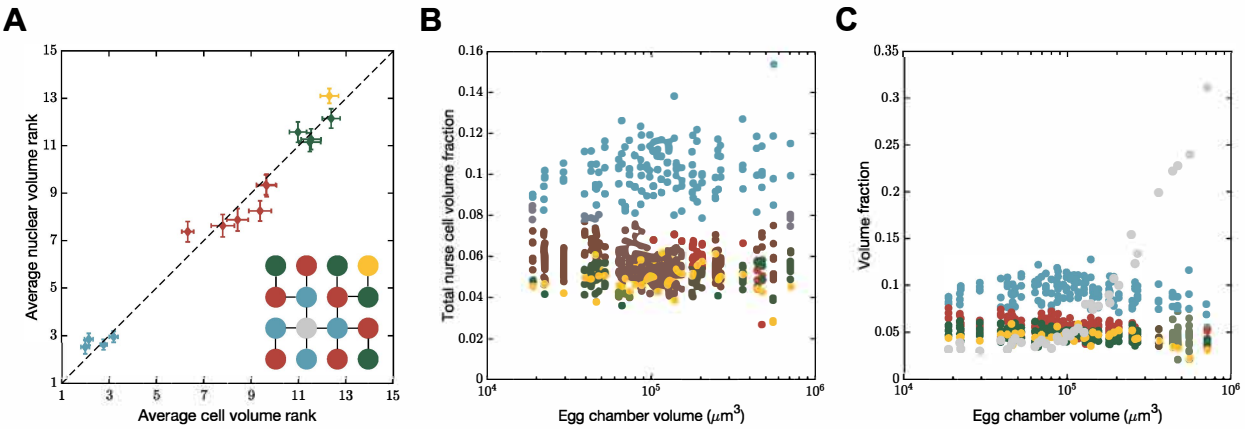

Fig. S1. Size divergences in the nurse cells and oocyte. (A) A plot of nuclear volume rank against cell volume rank shows the emergence of groups based on distance from the oocyte, and also demonstrates the deviation of the cells closest to the oocyte (n=40, R^2=0.976, error bars are s. d.). (B) Total nurse cell volume fraction (excludes the volume of the oocyte) as a function of egg chamber volume shows that across developmental stages, the cells closest to the oocyte are larger than the rest of the nurse cells, but this difference does not change through time (n=600 nurse cells from 40 egg chambers). (C) Volume fraction of cells against egg chamber volume highlights the onset of oocyte size divergence as the egg chamber progresses through oogenesis (n=640 cells from 40 egg chambers). All colors are based on proximity to oocyte, as denoted by the tree inset in (A) (gray depicts oocyte).